Appl. Phys. A 90, 123–127 (2008)
DOI: 10.1007/s00339-007-4281-5

Applied Physics A
Materials Science & Processing

Hot carrier photoluminescence in InN epilayers

M.D. YANG[1]
Y.P. CHEN[1]
G.W. SHU[1]
J.L. SHEN[1,✉]
S.C. HUNG[2]
G.C. CHI[2]
T.Y. LIN[3]
Y.C. LEE[4]
C.T. CHEN[5]
C.H. KO[5]

[1] Department of Physics, Center for Nanotechnology at CYCU and R&D Center for Membrane Technology, Chung Yuan Christian University, Chung-Li, Taiwan, R.O.C.
[2] Department of Physics, National Central University, Chung-Li 320, Taiwan, R.O.C.
[3] Institute of Optoelectronic Sciences, National Taiwan Ocean University, Keelung, Taiwan, R.O.C.
[4] Department of Electronic Engineering, Tung Nan Institute of Technology, Taipei, Taiwan, R.O.C.
[5] Department of Electrical Engineering, Yuan Ze University, Chung-Li, Taiwan, R.O.C.

Received: 23 March 2007/Accepted: 15 August 2007
Published online: 11 September 2007 • **© Springer-Verlag 2007**

ABSTRACT The energy relaxation of electrons in InN epilayers is investigated by excitation- and electric field-dependent photoluminescence (PL). From the high-energy tail of PL, we determine the electron temperature of the hot carriers. It was found that the electron temperature variation can be explained by a model in which the longitudinal optical (LO)-phonon emission is the dominant energy relaxation process. The LO-phonon lifetime is fitted to be 0.89 ps, which is higher than the theoretical phonon lifetime. This deviation is attributed to the presence of the non-equilibrium hot-phonon effects.

PACS 78.55.Cr; 78.66.Fd; 61.66.Fn; 78.20.Jq; 63.20.kd

1 Introduction

An understanding of the carrier relaxation in semiconductors is of fundamental interest in the physics of semiconductors as well as of importance in the design of high-speed devices and the evaluation of optical device performance [1–3]. The studies of hot carrier relaxation give information about the carrier–lattice and carrier–carrier scatterings because the carrier relaxation is directly related to inelastic collisions with the phonons and carriers. When excess energy is supplied to a carrier by optical excitation or an applied electric field, the energetic carrier becomes hot. The hot carriers then relax towards a less energetic state by two competing processes, namely scatterings with other carriers and emission of phonons [4]. The first process increases the temperature of the carriers, which are thermalized among themselves due to carrier–carrier scattering. The thermalized carriers then transfer energy to the lattice via phonon emission. Thus the carrier temperature can be determined by the interplay between the power supplied to the carriers by optical excitation or an applied electric field and the power loss from the carriers to the lattice via phonon emission.

InN has currently attracted a great deal of attention due to its potential application in semiconductor devices such as light-emitting diodes, lasers, high-speed electronics, and solar cells [5–8]. In recent years, there has been a considerable effort devoted to research on the optical and electronic properties of InN. However, there is little work concerning the hot carrier relaxation of InN. In this work, we study the excitation power and applied electric-field dependence of PL in InN epilayers in the medium excitation range ($\sim 10^{-13}$–10^{-11} W per electron). The high-energy tails of PL were characterized by effective electron temperatures that increase with increasing excitation intensity or electric field. The relationship between the electron temperature and the electron energy loss rate was compared with theoretical calculation based on the carrier-LO-phonons scattering. Under the medium excitation power, it is found that the main path of energy relaxation of the hot electrons is the LO-phonon emission in our InN with carrier concentrations of $4.5 \times 10^{18}\ \text{cm}^{-3}$.

2 Experiment

The sample investigated was grown on sapphire substrates by metalorganic vapor phase epitaxy (MOVPE). A low-temperature 20-nm GaN nucleation layer was firstly deposited at 500 °C, followed by a 2-μm GaN layer grown at 1000 °C. The substrate was then cooled to 600 °C to grow the InN. Trimethyl-indium (TMI) and NH_3 were used as sources and N_2 was used as the carrier gas at flow rates of 400, 18000, and 18 000 sccm for TMI, NH_3 and N_2, respectively. The pressure during growth was kept constant at 200 mbar. An InN layer with a thickness of 150 nm was grown on the GaN layer. The sample was further treated by rapid thermal annealing (RTA) in an N_2 environment. RTA was performed with an annealing time of 30 s and a ramp rate of 30 K/s at temperatures of 400 °C. RTA has been proven to be an effective technique to eliminate the nonradiative defects in InN and improve sample quality [6, 9]. The annealing results in a decrease of carrier concentration as well as a redshift and a line-width narrowing of PL band, which have been explained by a decrease of defects or impurities [6, 9]. Figure 1 shows the X-ray diffraction (XRD) pattern of the investigated InN epilayers. The InN(0002), GaN(0002), and sapphire(0006) diffraction peaks are observed at 31.5°, 34.8°, and 41.9°, respectively. It is noted that the In(101) peak does not appear around 33°, suggesting highly (0001) preferred orientation of the InN epilayers. The PL measurements were obtained using a focused Ar ion laser operating at a wavelength of 514.5 nm as the excitation source. Ohmic contacts of the sample were made by

✉ Fax: 886-3-2653299, E-mail: jlshen@cycu.edu.tw

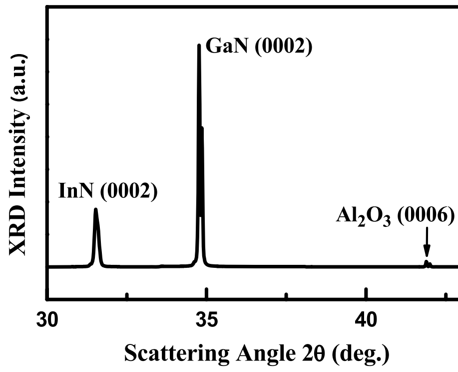

FIGURE 1 X-ray diffraction pattern of the studied InN epilayers

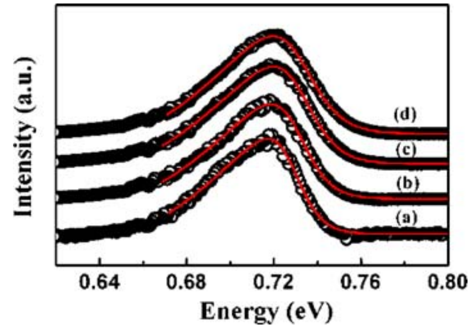

FIGURE 2 Measured (*circles*) and calculated (*solid line*) PL for the InN epilayers with different excitation density: (a) $50\,\mathrm{W/cm^2}$; (b) $85\,\mathrm{W/cm^2}$; (c) $250\,\mathrm{W/cm^2}$; (d) $380\,\mathrm{W/cm^2}$

indium (In) soldering, and the ohmic behavior was confirmed by the linear I–V characteristics. The sample was mounted in a close-cycle helium cryostat at temperature $T = 10\,\mathrm{K}$. The collected luminescence was dispersed by a 0.75-m spectrometer and detected with an extended InGaAs detector.

3 Results and discussion

In hot carrier PL, the photoexcitation of InN epilayers creates energetic electrons in the conduction band, which relax toward less energetic state by transferring energy to the lattice (via the electron–lattice scattering) and other electrons (via the electron–electron scattering). In the electron–lattice scattering, the electrons will cool by losing energy to the lattice through the collision with phonons. On the other hand, the electron–electron scattering is the collision of the energetic electron with a cooler electron, which results in a redistribution of energy among electrons in the electron gas. If the electron–electron collision rate is larger than the phonon emission rate, the non-equilibrium electron population in the electron gas relaxes towards a Maxwellian distribution and can be characterized by an electron temperature (T_e), which is higher than the lattice temperature (T_l) [4]. A critical carrier density n_c^* is defined for which the electron–electron collision rate is equal to the electron–phonon collision rate: [4]

$$n_c^* = \frac{8\pi(eE_0)(\hbar\omega_0)K^2\varepsilon_0}{e^4}\left[(N_q+1)\sinh^{-1}\left(\frac{\varepsilon-\hbar\omega_0}{\hbar\omega_0}\right)^{1/2} - N_q\sinh^{-1}\left(\frac{\varepsilon}{\hbar\omega_0}\right)^{1/2}\right], \quad (1)$$

where E_0 is an effective electric field, $\hbar\omega_0$ is the phonon energy, K is an average dielectric constant, ε_0 is the free-space permittivity, ε is the energy of the photoexcited electron, and N_q is the occupation number of phonon of wavevector q interacting with the electron. According to (1), the value of n_c^* in InN is calculated to be $9.06 \times 10^{18}\,\mathrm{cm^{-3}}$ for $T_l = 10\,\mathrm{K}$. For the electron density n much lower than n_c^*, the photoexcited electrons relax mainly by successive LO phonon emissions. As $n \sim n_c^*$, the electron gas then acquires a fraction of the excess energy through the electron–electron scattering: $W \sim \frac{n}{n+n_c^*}\Delta E_e$ [4].

The electron densities n of the investigated InN can be estimated from PL measurements [9]. The PL spectra of InN with four excitation power are shown in Fig. 2 for T_l at 10 K. The shape of PL bands in Fig. 2 was analyzed according to the following expression [6]:

$$I(\hbar w) \sim [\hbar w - E_g(n)]^{\gamma/2} f(\hbar w - E_g(n) - E_F)\,, \quad (2)$$

where is $\hbar w$ the photon energy, E_F is the Fermi energy of the degenerate electrons, n is the electron carrier concentration (expressed in $\mathrm{cm^{-3}}$), $E_g(n)$ is a carrier-concentration-dependent band gap that approaches the intrinsic band gap E_g at vanishing concentration, f is the Fermi–Dirac function, and γ is parameter involves the relaxation of the momentum conservation law in interband transitions ($2 \leq \gamma \leq 4$ for InN). The solid lines in Fig. 2 show the fitted PL spectra of InN according to (2), revealing a good agreement between the fitting curves and experimental data. Considering nonparabolicity of the electron band, the carrier concentration of the InN epilayers can be estimated the line-shape fitting [9]. Figure 3 shows carrier concentrations of the studied InN as a function of excitation power density. The carrier concentrations are within 4.5–$5 \times 10^{18}\,\mathrm{cm^{-3}}$ and the case $n \sim n_c^*$ in the previous paragraph should be considered.

Figure 4(a) shows the high-energy tail of PL for InN epilayers with the excitation power density at $90\,\mathrm{mW/cm^2}$. This tail exhibits an exponential dependence on the phonon energy and can be analyzed by the function [10]:

$$I(\hbar w) \sim \exp(-\hbar w/E_0)\,, \quad (3)$$

where E_0 is a specific energy. With low excitation power, E_0 reflects the sample quality at low temperatures (< 100 K for

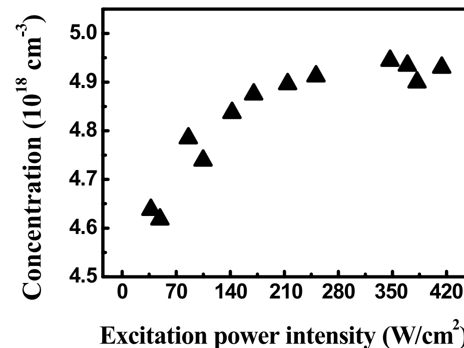

FIGURE 3 The electron concentration as a function of excitation power density

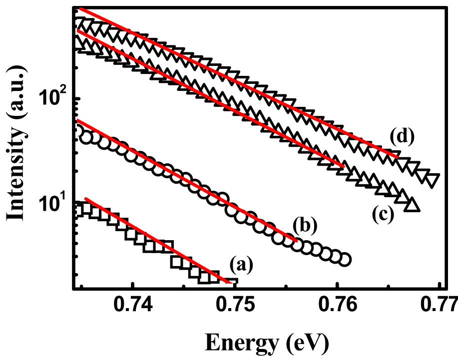

FIGURE 4 The high-energy tail of the PL for different excitation density: (a) 50 W/cm^2; (b) 85 W/cm^2; (c) 250 W/cm^2; (d) 380 W/cm^2. The *solid lines* display the slopes of the high-energy tail

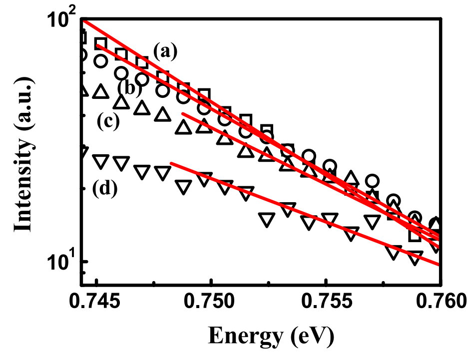

FIGURE 6 The high-energy tail of the PL for different applied electric field: (a) 1.3 V/cm; (b) 10 V/cm; (c) 15 V/cm; (d) 19 V/cm. The power density of the illuminated laser is 90 W/cm^2. The *solid lines* display the slopes of the high-energy tail

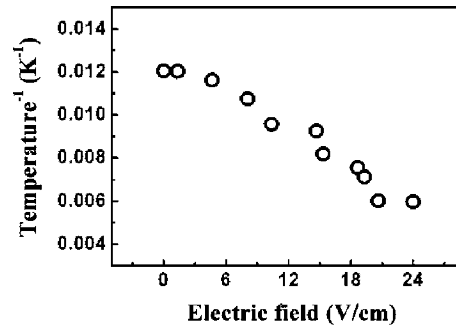

FIGURE 7 Inverse electron temperature versus applied electric field for the InN epilayers. The power density of the illuminated laser is 90 W/cm^2

InN) [10]. Using (3), we have fitted the high-energy tail of PL in Fig. 4(a). A value of 7.5 meV is obtained for E_0, indicating a good sample quality for the investigated InN epilayers. Figure 4(b)–(d) displays the high-energy tail of PL for another three different excitation densities. Each PL in Fig. 4(b)–(d) shows a high-energy tail that decreases also exponential with photon energy and can be fitted by (3). Under higher photoexcitation, E_0 can reflect the kinetic energy of the thermalized electrons and a well-defined T_e can be extracted. The inverse T_e versus the excitation power is plotted in Fig. 5. The slope of the inverse T_e, displayed as the solid line, corresponding to a value of 73 meV which is very close to the LO-phone energy in InN [11, 12]. The good agreement is an indication that the dominant energy loss mechanism for the electron gas is relaxation through the LO phonon emission. In other words, the LO phonon scattering is very efficient in transferring energy from electrons to the lattice.

The PL spectra of InN with four applied electric field (F) for T_l at 10 K are investigated. Figure 6 shows the high-energy tail of PL for the four different F with an excitation power density at 90 mW/cm^2. In this case, the electrons obtain excess energy from both illumination and electric field. However, as the applied electric field is large enough (> 10 V/cm) the dominant electron heating is due to the applied electric field. The slopes of the high-energy tails in Fig. 6 were also analyzed using (3) and the electron temperatures were obtained. With increasing F, the slope of the exponential tail decreases, leading to an increase of T_e. The inverse T_e versus the applied electric field F is plotted in Fig. 7. It is noted that the local T_l may increase by increasing F. To understand the effect of sample heating due to the applied electric field we analyzed the PL peak position under different F. Figure 8 displays the PL peak position as a function of F. The PL peak position remains unchanged with F from 0–15 V/cm, but redshifts as F increases further above 15 V/cm. The red-shift of the PL peak is due to combined effects of the field ionization of carriers, the Stark shift, and the energy-gap narrowing with increasing temperature. Suppose we neglect the Stark shift and consider the reduced electron concentrations as well as the energy-gap narrowing due to the increased temperature, T_l is estimated to be about 40 K at the largest F (30 V/cm). In a recent paper the relaxation of hot carriers through LO-

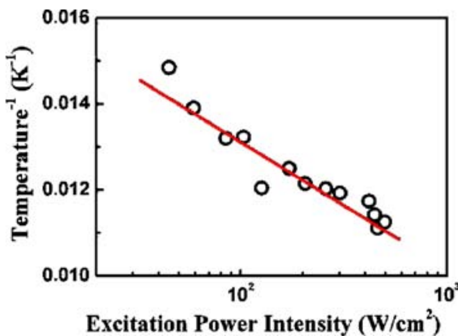

FIGURE 5 Inverse electron temperature versus excitation power density for the InN epilayers (*open circles*). The *solid line* corresponds to a slope where the activation energy equals to the LO-phonon energy (73 meV)

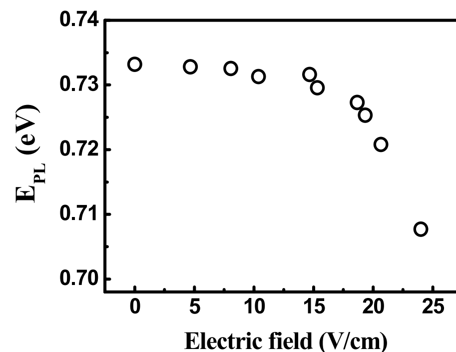

FIGURE 8 The PL peak position as a function of the applied electric field for InN epilayers

phonon in GaN is not affected by increasing the lattice temperature from 30 to 170 K [13]. Therefore we suggest that the LO phonon emission is still dominant for relaxation of the photoexcited electrons even T_l increases from 10 to 40 K.

In order to obtain the energy loss rate per electron from the experimental results we use the power balance equations. As the steady-state electron population increases by increasing excitation density, enhanced electron–electron scattering results in a larger fraction of the available energy being shared with the electron gas. Thus, the electron temperature T_e is determined by balancing the rate of generation for the energetic electrons with the rate of energy loss from the electrons to the lattice. For the photoexcitation, the pump power per electron P_e given to the electron is [4]

$$P_e = \frac{I}{d}\frac{W}{\hbar w}\frac{1}{n}, \tag{4}$$

where I is the laser power absorbed per unit area, d is the absorption length at laser energy, and W is the part of the photon excess energy obtained by electron. The open square in Fig. 9 displays the electron temperature as a function of the power input per electron (P_e). On the other hand, the power input per electron P'_e due to the applied electric field can be represented by

$$P'_e = \frac{iFL}{N}, \tag{5}$$

where i, L, and N are the current, sample length, and the total number of electrons, respectively. The electron temperature as a function of P'_e is shown as the open circles in Fig. 9.

The dominant process for this relaxation should be through LO phonon emission since the excess energy to be relaxed of about 1.87 eV is quite large. Assuming T_e is much larger than T_l, the energy-loss rate per electron due to the LO phonon scattering is given by [14]

$$P(T_e) = \left(\frac{E_{LO}}{\tau_{ph}}\right)\left(\frac{e^{x_0-x_e}-1}{e^{x_0}-1}\right)\left[\frac{e^{x_e/2}K_0(x_e/2)}{\sqrt{\frac{\pi}{x_e}}}\right], \tag{6}$$

where τ_{ph} is the effective LO-phonon lifetime, E_{LO} is the LO-phonon energy, $x_0 = \frac{E_{LO}}{k_B T_l}$, $x_e = \frac{E_{LO}}{k_B T_e}$, and K_0 is the modified Bessel function of order zero. In the steady state, the power input per electron is equal to the power loss to the lattice through phonon scattering. Taking values of 73 meV, 1.473 eV, 2.54 eV, 7.5×10^{-6} cm for E_{LO}, W, $h\nu_0$, d, respectively, the solid line in Fig. 9 displays the fitted T_e with the power loss per electron. It is found that the simple model based on the carrier scattering by LO phonon is able to explain the measured electron temperature variation with excitation power and applied electric field. In the calculations, τ_{ph} was fitted to be 0.89 ps. This value is about 42 times higher than the theoretical phonon lifetime $\tau_0 = 21$ fs, which can be obtained by [14]

$$\tau_0 = \left[\frac{e^2 E_{LO}}{2\pi\hbar^2}\left(\frac{m^*}{2E_{LO}}\right)^{1/2}\left(\frac{1}{\varepsilon_\infty} - \frac{1}{\varepsilon_s}\right)\right]^{-1}, \tag{7}$$

where m^* is the electron effective mass, ε_∞ and ε_s are the high frequency and static permittivities, respectively. This discrepancy is similar to those reported previously [14, 15]. The reason for disagreement between the fitted τ_{ph} and τ_0 was be attributed to the hot phonon effect caused by non-equilibrium phonon population that is created at high carrier density. This non-equilibrium phonon population slows down the hot electron cooling rate because the emitted LO phonons are reabsorbed by the hot electron gas. This reabsorption decreases the probability of phonon emission and the energy loss rate from electrons to the lattice. In our sample, carrier density is as high as 5×10^{18} cm^{-3}, the hot phonon effect should play a role in energy relaxation of the electron gas.

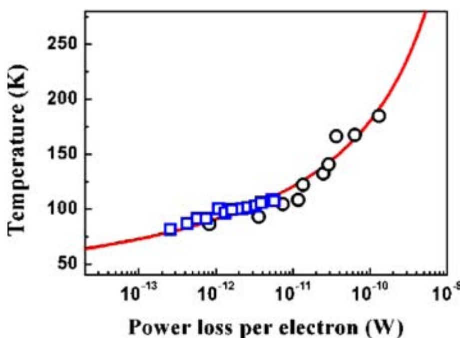

FIGURE 9 Electron temperature versus power loss per electron for InN epilayers. The *open squares* and (*circles*) are experimental data obtained from the excitation-power-dependent (electric-field-dependent) PL measurements. The *line* is a theoretical result according to (6)

4 Summary

In summary, the excitation power and applied-electric-field dependence of PL in InN epilayers was investigated. The high-energy tail of PL can be characterized by an effective electron temperature that increases with increasing excitation intensity and applied electric field. Under medium excitation density, it is found that the emission of LO phonons is the main energy loss process for electrons in our InN epilayers. The relationship between the electron temperature and the electron energy loss rate can be explained by a model based on the carrier scattering by LO phonons. From the fit, a phonon lifetime with a value of 0.89 ps is obtained, which is about 42 times of magnitude higher than the theoretical phonon lifetime. This deviation is attributed to the hot-phonon effect caused by non-equilibrium phonon population.

ACKNOWLEDGEMENTS This project was supported by the National Science Council under the grant numbers NSC 93-2112-M-033-010 and 93-2120-M-033-001, and the Center-of-Excellence Program on Membrane Technology, the Ministry of Education, Taiwan, R.O.C.

REFERENCES

1 T. Araya, N. Kato, N. Otsuka, J. Appl. Phys. **98**, 043 526 (2005)
2 Y. Lou, M. Yin, S. O'Brien, C. Burda, Electrochem. Soc. **152**, 427 (2005)
3 S.S. Prabhu, A.S. Vengurlekar, J. Appl. Phys. **95**, 7803 (2004)
4 J. Shah, Solid State Electron. **21**, 43 (1978)
5 V.Y. Malakhov, Proc. SPIE **3938**, 131 (2000)
6 V.Y. Davydov, A.A. Klochikhin, V.V. Emtsev, D.A. Kurdyukov, S.V. Ivanov, V.A. Vekshin, F. Bechstedt, J. Furthmuller, F. Aderhold, J. Graul, A.V. Mudryi, H. Harima, A. Hashimoto, A. Yamamoto, E.E. Haller, Phys. Stat. Solidi B **234**, 787 (2002)

7 A.G. Bhuiyan, A. Hashimoto, A. Yamamoto, J. Appl. Phys. **94**, 2779 (2003)
8 K.S.A. Butcher, T.L. Tansley, Superlatt. Microstruct. **38**, 1 (2005)
9 G.W. Shu, P.F. Wu, Y.W. Liu, J.S. Wang, J.L. Shen, T.Y. Lin, P.J. Pong, G.C. Chi, H.J. Chang, Y.F. Chen, Y.C. Lee, J. Phys.: Condens. Matter **18**, L543 (2006)
10 T. Stoica, R.J. Meijers, R. Calarco, T. Richter, E. Sutter, H. Lüth, Nano Lett. **6**, 1541 (2006)
11 V.M. Naik, R. Naik, D.B. Haddad, J.S. Thakur, G.W. Auner, H. Lu, W.J. Shaff, Appl. Phys. Lett. **86**, 201 913 (2005)
12 E. Kurimoto, M. Hangyo, H. Harima, M. Yoshimoto, T. Yamaguchi, T. Araki, Y. Nanishi, K. Kisoda, Appl. Phys. Lett. **84**, 212 (2004)
13 F. Binet, J.Y. Duboz, J. Off, F. Scholz, Phys. Rev. B **60**, 4715 (1999)
14 K. Wang, J. Simon, N. Goel, D. Jena, Appl. Phys. Lett. **88**, 022 103 (2006)
15 E. Ozturk, A. Straw, N. Balkan, G. Jones, J. Frost, D. Ritchie, Semicond. Sci. Technol. **7**, 1417 (1992)